Virtual Power Injection for Optimal Adjustment of Droop-Controlled Inverters

Matthew K. Chu Cheong
Department of Mechanical Engineering
The University of Texas at Austin
Austin, TX USA
mkchucheong@utexas.edu

Kaden E. Plewe
Department of Mechanical Engineering
The University of Texas at Austin
Austin, TX USA
https://orcid.org/0000-0002-8682-6879

Dongmei Chen
Department of Mechanical Engineering
The University of Texas at Austin
Austin, TX USA
dmchen@me.utexas.edu

Pengwei Du
Electric Regulation Council of Texas (ERCOT)
Austin, TX USA
Pengwei.Du@ercot.com

***Abstract*—As the penetration of inverter-based renewable energy sources increases, maintaining grid stability with a satisfactory frequency response will become more challenging. This needs to be addressed in order to maintain resilience to system disturbances while having desirable steady-state behavior. Among a variety of solutions proposed to compensate for the loss of system inertia, re-design of controllers could be very cost effective in mitigating the anticipated frequency deviations in the event of system disturbances. This paper proposes a novel method to virtually emulate inertial power compensation by modulating the behavior of a droop-controlled inverter. This is accomplished by adding a static output feedback controller to an otherwise conventionally droop-controlled voltage source inverter. This method provides additional degrees of freedom to optimize the primary response of a droop-controlled inverter to minimize the worst-case frequency deviation in the event of a sudden power loss. The design has been tested on a 14-bus and 24-bus power system to demonstrate that the proposed droop adjustment can substantially reduce the effect of sudden power imbalances on frequency response with a minimal increase in the energy cost.**

Keywords*—Virtual power injection, H-infinity optimization, power system control, low-inertia power grid

I. Introduction

Microgrids, renewable power generators, and distributed generation units in general are becoming more widely developed and are expected to play an increasing role in future electricity markets [1]–[4]. Despite having advantages with respect to efficiency, renewable penetration, and economics, an inverter-dominant power grid could be more sensitive to the power imbalance due to the disturbances caused by distributed generators and dynamic loads. Challenges arise in the realm of uncertainty, logistical responsibility, control, and market management [2], [3], [5]. These challenges are directly attributed to the integration of inverter-based generators electronically coupled to the grid, which often operate in a plug-and-play fashion.

Traditional electrical grids are primarily connected by centralized, large-size power plants that generate electricity with large synchronous generators (SGs). These generators are high-inertia devices and have a damping effect for the frequency oscillations induced by the disturbances via load or supply variations, grid faults, or unexpected load changes [6], [7]. In modern power grids, a higher proportion of distributed generators are instead connected to the grid through an inverter and thus reduce the system inertia, which diminishes the overall inertial resilience. This also poses a major technical problem for microgrids, where the proportion of inertia-less generation may be sufficiently high to destabilize the grid [8], broadly inhibiting the development of such systems.

Using batteries to improve the frequency response for a future power grid has been proposed, but it is prohibitively expensive. The desirable inertia of synchronous generators can be alternatively emulated by virtual inertia devices enabled as supervisory control algorithms for inverters [9]. The most popular inertia emulation approaches can be clarified as two categories: 1) using a physics-based approximation to control power converters in a way that mimics virtual synchronous generators (VSG) and 2) using a droop control that autonomously controls the power injection to mitigate voltage and frequency deviations from their nominal values. Though the mathematical equivalence of the VSG emulation methods and droop-based methods has been demonstrated in [10] and [11], there are notable differences in the dynamic behavior of converters that deploy either method [12].

For the first category, the power swing equation is a commonly used approximation for the damping and inertial effects of SGs. Sakimoto et. al. successfully emulated the inertial response of SGs by implementing the swing equation as a governor control input for asynchronous devices in [13]. The most recent advancements in this swing-equation based approach were presented in [14] and [15], where the inertial and damping gains are adaptively tuned to balance the dual objectives of frequency synchronization and energy conservation through a novel Linear Quadratic Regulator (LQR)-based approach.

For the second category, several approaches have been proposed to modify the droop control law to improve its transient performance. In [16] and [17] additional derivative and integral droop characteristics are added to modify the transient response. Another host of modified droop controllers are featured by the adaptive or interval-based approach, where droop gains are tuned in a modular way to add flexibility over the expected operational domain. An interval-based approach was introduced in [18], where the real power droop control law is modified based on the

inverter's output voltage triggers. A similar adaptive approach can be applied through droop gain scheduling, as is shown in [19], where additional adaptive droop gains are used to influence the stability and resilience of individual inverters.

These aforementioned methods share the intention of improving the transient response of inverter-connected distributed energy resources (DERs). However, they either are designed for the operation of a single inverter without considering the system-wide impact, or focus on transient control using a control signal proportional to the time-derivative of a measurement, which may be susceptible to the measurement noise. This paper takes a different approach in that the proposed control action is a function of all available local measurements, each with its individual gain; rather than having a control signal proportional to the derivative, our proposed control is independently constrained to be zero at steady-state. In this way, it can modify only the transient component of the response, and thus emulating a more inertial response at steady-state. Another salient feature of the proposed method is that we are afforded more degrees of freedom for control tuning. These degrees of freedom are then leveraged for optimal control, where the control gains are rigorously synthesized by optimizing the transient performance of the full network model. This intrinsically allows the resulting controller to account for the behavior of other controlled sources during operation.

Building upon our previous work [20], [21], this paper presents a novel method of virtual power injection that allows voltage source inverter (VSI) droop controllers to be adjusted via static output feedback (SOF) control. These controllers are synthesized to minimize the H-infinity norm of the transfer function between an exogenous input and selected controlled outputs. In this paper, we explore how H-infinity modulation can be used in the context of virtual inertia emulation. The H-infinity class of controllers is considered advantageous over other optimal control methods because it naturally extends to the idea of worst-case disturbance rejection. This characteristic is desirable for power systems, where the focus is on maintaining system tolerances and safety conditions by mitigating the largest disturbance. H-infinity controllers allow us to optimize for these worst-case situations, unlike the quadratic optimization (e.g. H-2 control) which may be more useful for quantities we wish to optimize over time, such as efficiency. Here the primary focus is to immediately stabilize the grid frequency following a disturbance, thus motivating H-infinity control.

The key contribution of this paper is the new control design to modulate the transient behavior of droop-controlled voltage source inverters to emulate a more stable and damped inertial response. It is done by the application of virtual power injection for optimally adjusting the droop characteristic of voltage source inverters. The resulting controller is decentralized in the sense relative to conventional droop control. It requires no additional real-time data for improved performance; offline controller synthesis incorporates the full network model in order to optimize the response without requiring network-wide measurements during real-time operation. The optimal selection of the droop characteristic is done via the H-infinity control technique, which is used to optimally select the control gains, resulting in a novel decentralized model-based optimal approach for the emulation of inertial characteristics by inverter-connected power sources. In particular, we highlight the application in a power system, where inertia-less generation from a combination of renewable sources and battery-energy-storage-systems are likely to comprise a more significant proportion of the power supply.

The following sections describe the modeling, model reduction and controller synthesis, simulation, and testing results. The autonomous model that is used for controller synthesis and for simulating the test cases is described in Section II; this is generally a summary of existing modeling practices. The model adjustment and model-reductive methodology to facilitate SOF control synthesis and the associated control methodology design is presented in Section III; this section highlights the novel design contribution of this paper. The test case that is used to validate the performance of the proposed microgrid control methodology is provided in Section IV. Finally, the results are presented and discussed in Section V and conclusions are made in Section VI.

II. Power Grid Model

The power grid model considered here consists of a network of interconnected grid-forming distributed energy resources (DER) and dynamic loads. The modeling framework used here follows from [22]. Within the modeling framework, n buses are connected through inductive-resistive distribution lines in a system with k generators that are electronically coupled to the power grid via voltage source inverters (VSI). The model of an individual sub-system and adjacent connections is depicted in Fig. 1. The dq0 reference frame transformation is used to convert a three-phase AC system described by (a, b, c) to two synchronously rotating DC components (d, q, ω), where ω is the angular frequency at which the two DC components rotate.

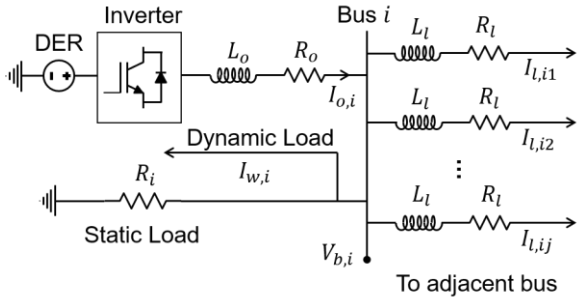

Fig. 1. Circuit diagram for an individual grid-forming sub-system model.

The complete autonomous power grid model contains k grid-forming inverters that operate with a droop controller and $n-k$ load-only buses that are all connected by h bus-to-bus distribution lines. The full power grid model considers the inverter state variables, Δx_g, and the network state variables, Δx_{net}. Hence, the state variables for the full autonomous power grid model, $\Delta x \in \mathbb{R}^{(6k+2h)}$, are

$$\Delta x = [\Delta x_{g,1}, \Delta x_{g,2}, \dots, \Delta x_{g,k}, \Delta x_{net}]^T, \qquad (1)$$

where

$$\Delta x_{g,i} = \left[\Delta\omega_i, \Delta\delta_i, \Delta P_i, \Delta Q_i, \Delta I_{o,i,d}, \Delta I_{o,i,q}\right], \quad (2)$$

and

$$\Delta x_{net,ij} = [\Delta I_{l,ij,D}, \Delta I_{l,ij,Q}\,]. \quad (3)$$

The autonomous power grid model can then be written as

$$\Delta\dot{x} = A_{ol}\Delta x + G_{ol}w, \quad (4)$$

where $A_{ol} \in \mathbb{R}^{(6k+2h)\times(6k+2h)}$ is the open-loop state matrix and $G_{ol} \in \mathbb{R}^{(6k+2h)\times 2}$ is the disturbance input matrix for $w \in \mathbb{R}^2$, which drives the dynamic load current at each node:

$$w \coloneqq [\Delta I_{w,d}, \Delta I_{w,q}]^T. \quad (5)$$

III. Controller Design

The overarching theme of the proposed control design is to adjust the droop-controlled inverter to optimally stabilize its transient disturbance response. In this context, the advantage of an inertial response is that the inertial energy compensation dampens this transient response. Our proposed control design intends to emulate this process.

There are two distinct differences between inverter-connected DER's and synchronous generators: (1) inverters have no inertial energy available and (2) the power response of an inverter-connected DER is much faster than a synchronous generator. Accordingly, this design centers on controlling the VSI to act as though there is a secondary power source available to optimize the transient response. However, instead of injecting real or reactive power from a secondary power source, we adjust the controlled inverter behavior to induce the same effect at a lower cost. For this reason, we refer to this method as virtual power compensation.

This section describes the sequential steps taken to design this controller. Section III-A details the overall structure of the controller, Section III-B outlines the model reductive steps taken for control design and numerical stability, and Section III-C briefly summarizes the H-infinity controller gain synthesis for network-wide optimization.

A. Virtual Power Compensation

Virtual power compensation is implemented by modifying the real and reactive power inputs to the droop controller, P and Q, respectively. Droop control is based on a proportional gain relative to these power measurements. The proposed design instead works with the modified quantities, $\widehat{P}$ and $\widehat{Q}$:

$$\begin{aligned} \widehat{P} &\coloneqq P - P_v \\ \widehat{Q} &\coloneqq Q - Q_v, \end{aligned} \quad (6)$$

where P_v and Q_v are added control variables that are set to behave as virtual power. In this formulation, the controlled inverter operates according to a conventional droop characteristic, where the input real and reactive powers are simply $\widehat{P}$ and $\widehat{Q}$ instead of the measured P and Q. Note that P_v and Q_v are not constrained to be nonnegative, so the sign is merely a convention. The resulting droop characteristic is

$$\begin{aligned} \Delta\omega &\coloneqq -m_p\left(\widehat{P} - P^*\right) \\ \Delta V_d &\coloneqq -n_q\left(\widehat{Q} - Q^*\right). \end{aligned} \quad (7)$$

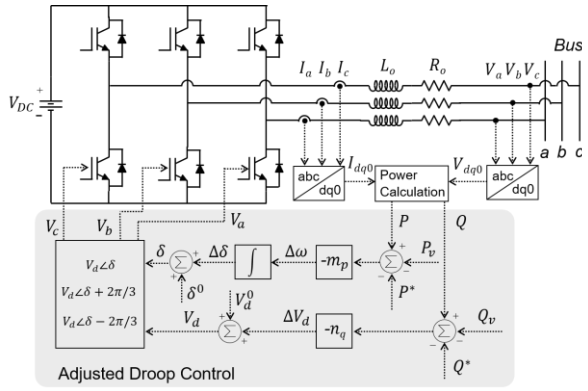

Fig. 2. Diagram of the adjusted droop controlled VSI with a virtual power injection implementation.

By constraining P_v and Q_v to be zero at steady-state, the proposed design maintains the steady-state behavior of conventional droop control. This is implemented by augmenting the system dynamics with the controlled state variables U_P and U_Q:

$$\begin{aligned} \dot{U}_p &= P_v \\ \dot{U}_Q &= Q_v. \end{aligned} \quad (8)$$

An augmented state vector, $\Delta\hat{x}_g \in \mathbb{R}^8$, representing the sub-system model that includes (8) is given by

$$\Delta\hat{x}_g = \left[\Delta\omega, \Delta\delta, \Delta P, \Delta Q, \Delta I_{o,d}, \Delta I_{o,q}, U_P, U_Q\right]. \quad (9)$$

The resulting dynamic system is controlled to be stable, and so all time-varying quantities are constant at steady-state:

$$\begin{aligned} \dot{U}_{P,ss} &= 0 = P_{v,ss} \\ \dot{U}_{Q,ss} &= 0 = Q_{v,ss}. \end{aligned} \quad (10)$$

This ensures that as the transient dynamics decay, the steady-state inputs to the droop controller are unchanged:

$$\begin{aligned} \widehat{P} \to P \quad &\text{as} \quad \hat{x}_g \to \hat{x}_{g,ss} \\ \widehat{Q} \to Q \quad &\text{as} \quad \hat{x}_g \to \hat{x}_{g,ss}\,. \end{aligned} \quad (11)$$

The added virtual power injection control variables, $u \in \mathbb{R}^{2k}$, which are defined as

$$u \coloneqq [P_{v,1}, Q_{v,1}, P_{v,2}, Q_{v,2}, \ldots, P_{v,k}, Q_{v,k}]^T, \quad (12)$$

situate the power grid model in a way that allows SOF methods to be exercised. The updated state variables are

$$\Delta\hat{x} = [\Delta\hat{x}_{g,1}\,, \Delta\hat{x}_{g,2}\,, \ldots, \Delta\hat{x}_{g,k}\,, \Delta x_{net}]^T, \quad (13)$$

and the corresponding system is formulated as

$$\begin{aligned} \Delta\dot{\hat{x}} &= A\Delta\hat{x} + Bu + Gw \\ z &= C_z\Delta\hat{x} + D_z u, \end{aligned} \quad (14)$$

where $A \in \mathbb{R}^{(8k+2h)\times(8k+2h)}$ is the full-model state matrix that follows from the formulated governing equations, $B \in$

$\mathbb{R}^{(8k+2h)\times 2k}$ is the virtual power injection control input matrix and $G \in \mathbb{R}^{(8k+2h)\times 2}$ is the disturbance input matrix. The controlled output, z, is designed to be weighted appropriately for H-infinity controller synthesis by selecting a sufficient C_z and D_z, and will be described in Section III-C.

B. Model Reduction for Controller Synthesis

The modeled power grid dynamics present conspicuously different timescales, making this a stiff dynamic system. This results in poor numerical conditioning that leads to numerical instability during controller synthesis, especially as the scale of the model grows. This section describes these timescale variations, as well as the reduced-order model used to solve this problem during the controller design process.

The characteristic timescale associated with the inverter output currents, I_o, and the line currents, I_l, is that of a standard R-L circuit, $\tau_{RL} = L_o/R_o \approx 10^{-4}$. This is several orders of magnitude faster than the time response associated with the droop-controlled inverter response. The inverter responds to measurement signals that are filtered via a low-pass filter, with a characteristic time scale on the order of $\tau_f \approx 10^{-2}$.

The low-pass filtered dynamics lead to distinct timescale separations in the full model. A classical approach to addressing this issue is to separate control loops for faster and slower dynamics. This scenario is distinct in that the slower dynamics are associated with the local subsystems, while the network interconnections are associated with faster dynamics. A goal of the proposed design is that control actuation on the local subsystem level should be optimal with respect to network interconnections, and so a complete timescale separation during the design process would not be feasible.

Instead, the model is reformulated so that the fast R-L dynamics are treated as quasi-steady-state and reduced to algebraic relationships. The remaining slower states are retained as dynamic state variables. In this way, the network information is retained in the reduced model via the algebraic relationships from the faster network variables, while removing a source of numerical instability due to timescale magnitudes.

Formally, the faster variables are set to remain at their steady-state

$$\frac{d\hat{x}_f}{dt} = 0 \qquad \forall t \geq 0. \tag{15}$$

For a single grid-forming subsystem at Bus i the linearized slow state variables, $\Delta\hat{x}_{s,i} \in \mathbb{R}^6$, and fast state variables, $\Delta\hat{x}_{f,i} \in \mathbb{R}^2$, are separated as follows:

$$\Delta\hat{x}_{s,i} = [\Delta\omega_i, \Delta\delta_i, \Delta P_i, \Delta Q_i, U_{P,i}, U_{Q,i}] \tag{16}$$

and

$$\Delta\hat{x}_{f,i} = [\Delta I_{o,i,d}, \Delta I_{o,i,q}]. \tag{17}$$

All line currents in the complete power grid model are also included in the fast state representation. Hence, the state variables for the complete model can be separated according to

$$\Delta\hat{x}_s = \left[\Delta\hat{x}_{s,1}, \Delta\hat{x}_{s,2}, \ldots, \Delta\hat{x}_{s,k}\right]^T \tag{18}$$

and

$$\Delta\hat{x}_f = \left[\Delta\hat{x}_{f,1}, \Delta\hat{x}_{f,2}, \ldots, \Delta\hat{x}_{f,k}, \Delta x_{net}\right]^T. \tag{19}$$

With the states separated in this way, the linear power grid model dynamics can be represented in block form as

$$\begin{bmatrix}\Delta\dot{\hat{x}}_s \\ 0\end{bmatrix} = \begin{bmatrix}A_s & A_{sf} \\ A_{fs} & A_f\end{bmatrix}\begin{bmatrix}\Delta\hat{x}_s \\ \Delta\hat{x}_f\end{bmatrix} + \begin{bmatrix}B_s \\ B_f\end{bmatrix}u + \begin{bmatrix}G_s \\ G_f\end{bmatrix}w, \tag{20}$$

where $A_s \in \mathbb{R}^{6k\times 6k}$, $A_{sf} \in \mathbb{R}^{6k\times 2(k+h)}$, $A_{fs} \in \mathbb{R}^{2(k+h)\times 6k}$, and $A_f \in \mathbb{R}^{2(k+h)\times 2(k+h)}$ are the reduced state matrices, $B_s \in \mathbb{R}^{6k\times 2k}$ and $B_f \in \mathbb{R}^{2(k+h)\times 2k}$ are the separated input matrices for the virtual power injection control input, and $G_s \in \mathbb{R}^{6k\times 2}$ and $G_f \in \mathbb{R}^{2(k+h)\times 2}$ are the separated disturbance input matrices.

From (20) an algebraic representation for $\Delta\hat{x}_f$, dependent on $\Delta\hat{x}_s$, u and w, is obtained:

$$\Delta\hat{x}_f = -A_f^{-1}(A_{fs}\Delta\hat{x}_s + B_f u + G_f w). \tag{21}$$

The fast state matrix, A_f, is an invertible matrix by design since $\Delta\hat{x}_f$ contains a set of current variables for independent power grid network lines. The augmented quasi-steady-state model can be represented by substituting $\Delta\hat{x}_f$ into the differential equation for the slow variables to obtain

$$\Delta\dot{\hat{x}}_s = A_r\Delta\hat{x}_s + B_r u + G_r w, \tag{22}$$

where

$$\begin{aligned} A_r &= A_s - A_{sf}A_f^{-1}A_{fs} \\ B_r &= B_s - A_{sf}A_f^{-1}B_f \\ G_r &= G_s - A_{sf}A_f^{-1}G_f. \end{aligned} \tag{23}$$

The reduced linearized power grid model that can be used in the synthesis of an optimal feedback controller, $K_r \in \mathbb{R}^{2k\times 6k}$, can now be written as

$$\begin{aligned} \Delta\dot{\hat{x}}_s &= A_r\Delta\hat{x}_s + B_r u + G_r w \\ z &= C_{z,s}\Delta\hat{x}_s + D_z u. \end{aligned} \tag{24}$$

C. H-infinity Controller Synthesis

The formulation of the full-information power grid model that is described in Section III-A and III-B presents an opportunity to apply optimal control techniques, where the transient system response can be improved by optimally controlling the virtual power injection inputs. In this paper, we are interested in minimizing the effect that the set of dynamic load disturbances, w, have on the controlled output, z. With the problem objective defined in this way, an intuitive approach is to use H-infinity methods to minimize the H-infinity norm of the transfer function, $T_{wz}(s)$. This transfer function summarizes the input-output relationship that the disturbances have on the system. The H-infinity controller synthesis that is used in this paper achieves these desired goals and produces a stabilizing feedback controller, K_r, for use in the closed-loop system.

Evaluation of H-infinity SOF developments for microgrids can be found in Bevrani [23]. Comprehensive development of the LMI conditions used in the synthesis of the sub-optimal H-infinity convex programming problem is introduced in Boyd et. al. [24], Crusius and Trofino [25] and Rubió-Massegú et. al. [26].

The H-infinity norm is evaluated for the closed-loop reduced-order power grid model which can be written as

$$\begin{aligned} \Delta\dot{\hat{x}}_s &= A_{r,cl}\Delta\hat{x}_s + G_s w \\ z &= C_{z,s,cl}\Delta\hat{x}_s, \end{aligned} \tag{25}$$

where

$$\begin{aligned} A_{r,cl} &= A_r + B_r K_r \\ C_{z,s,cl} &= C_{z,s} + D_z K_r. \end{aligned} \tag{26}$$

Minimizing the H-infinity norm of the transfer function from w to z, $\|T_{wz}(s)\|_\infty$, effectively accomplishes the goal of minimizing the selected controlled outputs in z when the system is perturbed by a dynamic load disturbance, w. Here, it is not necessary to find an explicit minimum for $\|T_{wz}(s)\|_\infty$. The problem, instead, can be cast with a sub-optimal supremum objective such that

$$\|T_{wz}(s)\|_\infty < \gamma \tag{27}$$

is satisfied, where the strict upper bound, γ, is minimized. The attainment of a controller, K_r, that minimizes the upper bound and stabilizes the closed-loop system is achieved by formulating a constrained convex programming objective for decentralized H-infinity control and solved using open-source convex optimization solvers [27], [28]. The problem is formulated as an LMI with γ as a constrained parameter to obtain decentralized controllers for each inverter that satisfy (27) using a similar approach to what was presented in [26]. Specifically, it has been shown that $K_r = YX^{-1}$ satisfies (27) when γ is minimized with the following constraints:

$$\begin{bmatrix} A_r X + X A_r^T + B_r Y + Y^T B_r^T + \gamma^{-2} G_r G_r^T & * \\ C_{z,s}X + D_z Y & -I \end{bmatrix} < 0 \tag{28}$$

where $*$ signifies a symetric entry, $\gamma > 0$, and $X > 0$ and Y are unknown matrices of compatible dimensions. The resulting optimal controller, K_r, can then be implemented as a standard feedback controller in the full-state model using

$$u = [K_r \quad \mathbf{0}] \begin{bmatrix} \Delta\hat{x}_s \\ \Delta\hat{x}_f \end{bmatrix} \tag{29}$$

Although K_r is synthesized with the full model, we pose the problem such that K_r takes the block diagonal form

$$K_r = \begin{bmatrix} K_{r,1} & \mathbf{0} & \cdots & \mathbf{0} \\ \mathbf{0} & K_{r,2} & & \\ \vdots & & \ddots & \vdots \\ \mathbf{0} & & \cdots & K_{r,k} \end{bmatrix} \tag{30}$$

by restricting X and Y to both be block diagonal matrices of proper dimensions. Recalling that $K_r = YX^{-1}$, the sparsity pattern of K_r can be set arbitrarily, as it will always match the sparsity pattern of Y if X is of block diagonal form.

This property is of particular interest when applied to power grid typologies because there can be a large cost gap between centralized and decentralized controllers. By setting K_r to be of block diagonal form, the controllers can be deployed to their respective inverters and only require local state information. This eliminates the need for real-time communication between all of the inverters in the topology.

D. Controller Weighting

The controlled output variables that are designated in the reduced model formulation are the angular frequency, ω, virtual injected real and reactive power, P_v and Q_v, and the integrated virtual injected real and reactive power, U_P and U_Q. The actuation effect of each variable in z changes the closed-loop dynamic response of the system. In general, varying the weight of ω, U_P and U_Q adjusts the damping of the transient response and adjusting the weight of P_v and Q_v adjusts the overall control effort of the corresponding inverter. The weights of these variables are adjusted in $C_{z,s}$ and D_z for an individual grid-forming inverter, i, using the following definitions:

$$\begin{aligned} C_{z,s,i} &:= \begin{bmatrix} \beta_\omega & 0 & 0 & 0 & 0 & 0 \\ 0 & 0 & 0 & 0 & 0 & 0 \\ 0 & 0 & 0 & 0 & 0 & 0 \\ 0 & 0 & 0 & 0 & \beta_P & 0 \\ 0 & 0 & 0 & 0 & 0 & \beta_Q \end{bmatrix}_{5\times 6} \\ D_{z,i} &:= \begin{bmatrix} [0 & \alpha_{P2}V_q^0 & \alpha_{P1}V_d^0 & 0 & 0 \\ 0 & \alpha_{Q2}V_q^0 & \alpha_{Q1}V_d^0 & 0 & 0 \end{bmatrix}^T_{2\times 5.} \end{aligned} \tag{31}$$

and the full-scale reduced controlled output matrices are constructed as block matrices according to

$$\begin{aligned} C_{z,s} &= \mathrm{diag}\left\{C_{z,s,1}, C_{z,s,2}, \ldots, C_{z,s,k}\right\} \\ \mathrm{D_z} &= \mathrm{diag}\left\{D_{z,1}, D_{z,2}, \ldots, D_{z,k}\right\}. \end{aligned} \tag{32}$$

With the controlled output matrices constructed in this way, the controlled output that is considered in the H-infinity synthesis for each grid-forming inverter, i, is

$$z_i = [\beta_\omega \Delta\omega_i, \alpha_P P_{v,i}, \alpha_Q Q_{v,i}, \beta_P U_{P,i}, \beta_Q U_{Q,i}]^T. \tag{33}$$

For the results presented in this paper, the weighting parameters in $C_{z,s}$ and D_z were identical for all inverters and are listed in TABLE I. In reality, the decentralized control strategy would benefit from an optimal selection of $C_{z,s}$ and D_z to better counteract disturbances at any location in the microgrid network. The pursuit of a formal weight-selection methodology is left as an open problem for future investigation.

TABLE I. WEIGHTING PARAMETERS

β_ω	β_P	β_Q	α_{P1}	α_{P2}	α_{Q1}	α_{Q2}
1.25	100	100	1	10	10	-10

IV. SIMULATION

The topology of the simulated power grid system is adapted from the IEEE 14-bus and 24-bus bulk power grid test systems [29], which are a representation of portions of the American Electric Power System in the Midwestern United States. The general behavior and transient stability of the IEEE topologies has been studied previously [30], [31]. The network topology (i.e. configuration and number of connections, buses, and generators), shown in Fig. 3, is consistent with the IEEE designs.

For the test case that is studied in this paper, a simplified configuration is considered, where all generators have the same capacity and the distribution line inductance for every interconnection is identical. The parameters for the test case system are provided in TABLE II. and are consistent with those used in [22] and [32]. The comparison metrics used

here are described in Section IV-A and identified in Fig. 5 and Fig. 4.

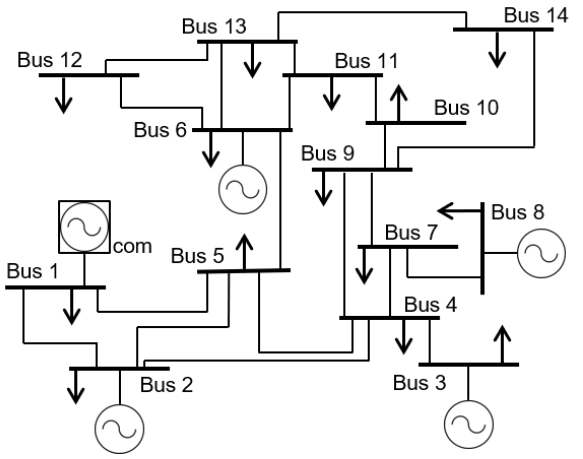

(a)

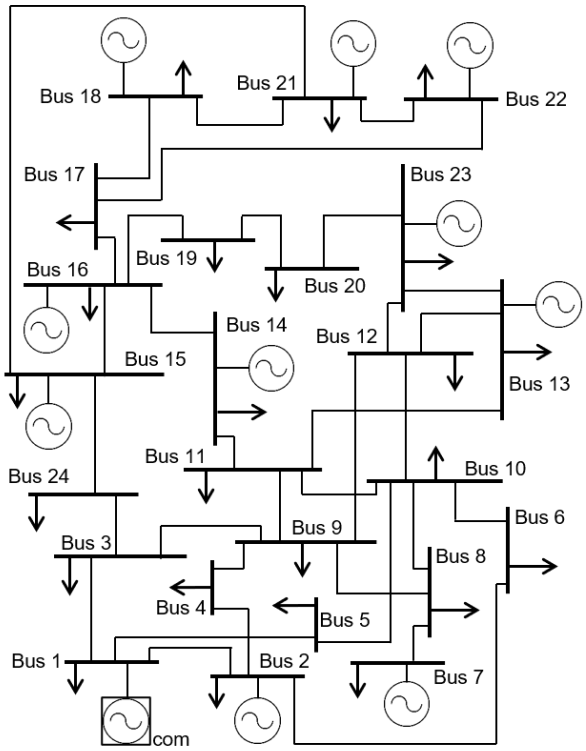

(b)

Fig. 3. Modified IEEE 14-bus (a) and 24-bus (b) test systems used for simulating a transient response to sudden load shifts at individual buses. The common reference bus used for these simulations is indicated by the $[\cdot]_{com}$ at Bus 1.

A. Performance Metrics

The performance metrics that were chosen for this study quantify and compare transient resilience and stability for the proposed control design relative to traditional droop control. The H-infinity norm is used as a measure for worst-case performance.

TABLE II. SYSTEM PARAMETERS

Description	Symbol	Value	Unit
Base Apparent Power	S_{base}	6000	W
Base Voltage	V_{base}	380	V
Base Frequency	f_{base}	60	Hz
Inverter Output Resistance	R_o	0.0042	p.u.
Inverter Output Reactance	X_o	0.0208	p.u.
Line Resistance	R_l	0.0125	p.u.
Line Reactance	X_l	0.0125	p.u.
Load Resistance	R	0.4155	p.u.
Load Reactance	L	0.0831	p.u.
Disturbance Load Change	ΔI_w	0.05	p.u.

The comparison of the traditional and adjusted droop control methods is built on four metrics taken with respect to frequency: 1) The change in peak undershoot, ΔM_p, 2) change in the network settling time, $\Delta\tau_s$, 3) change in peak system variance, $\Delta\sigma_p^2$, and 4) change in the integrated system variance, $\Delta\int\sigma^2$. The peak undershoot of the system response is a measure of the maximum frequency deviation from the final steady-state value, and the settling time quantifies the time required for the frequency at every bus to stabilize at $\pm 5\%$ of the final steady-state value. These two metrics are computed for each grid-forming inverter, and the values for the inverter with the largest deviation and longest settling time, respectively, are reported. Metrics (3) and (4) quantify the synchronization of the full power grid by considering the time-varying variance across all inverter frequencies:

$$\sigma^2(t) = \frac{1}{k-1}\sum_{i=1}^{k} |\Delta\omega_i(t) - \Delta\overline{\omega}(t)|^2. \qquad (34)$$

Finally, the change in total energy input, $\Delta\int\Delta S$, is quantified by integrating the apparent power supplied over the settling period.

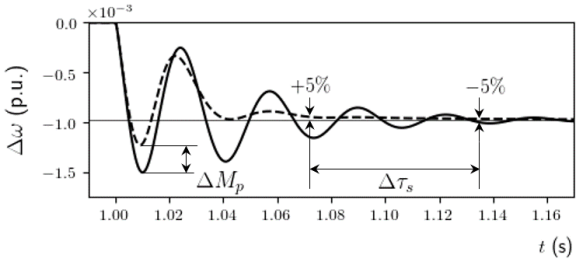

Fig. 5. Example of angular frequency metrics used to quantify the change in transient performance for the microgrid system with adjusted droop control (dashed line) versus traditional droop control.

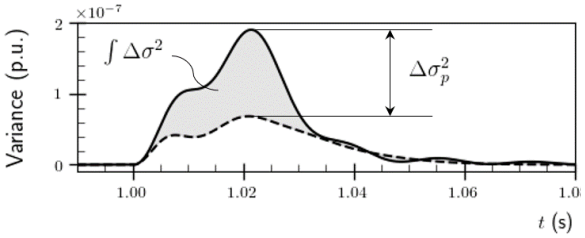

Fig. 4. Comparison of variance for traditional droop control and full-order adjusted droop control (dashed line).

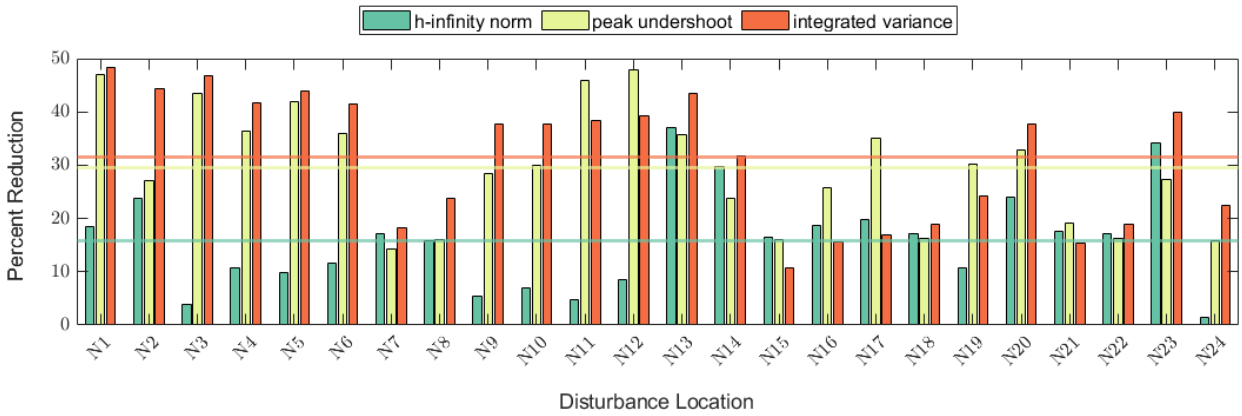

Fig. 6. Percent reduction in H-infinity norm, peak undershoot, and integrated variance under isolated disturbance scenarios at each bus. Horizontal lines represent the average value of corresponding metrics.

V. Results and Discussion

The transient performance and resilience of the power grid typologies in response to a sudden dynamic load shift is evaluated using the system and metrics described in Section IV. First, the disturbance is simulated as a 5% load increase [33] relative to the steady-state power draw at Bus 1, and is applied instantaneously at $t = 1s$ to initiate the transient response of the IEEE 14-Bus test system. The results for this simulation are shown in Fig. 7 and listed in TABLE I. In order to demonstrate the added resilience to disturbances at any location in a given topology, the same 5% load increase is applied at every bus in the IEEE 24-Bus topology as separate events. The results for these simulations are shown in Fig. 6.

Fig. 4 shows the total variance (Eq. 35) between the frequency at the five grid-forming inverters as the system is stabilized. There is a significant improvement in synchronization during the transient period–quantified by the 64.19% and 51.94% reduction in peak and integrated variance, respectively.

TABLE III. Performance Metric Evaluation for IEEE 14-Bus Simulation with a Disturbance at Bus 1 (P.U. Basis)

Controller	$\|T(s)\|_\epsilon$	M_p	τ_s	σ_p^2	$\int \sigma^2$	$\int \Delta S$
Traditional	1.583	-5.245 e-4	1.069 e-1	1.901 e-7	4.024 e-5	2.228 e-2
Adjusted	1.017	-0.944 e-4	0.741 e-1	0.681 e-7	1.934 e-5	2.288 e-2
Δ (%)	-35.75	-82.00	-30.68	-64.18	51.94	2.69

The transient response of the system is shown in Fig. 7, where the angular frequency and apparent power injection for grid-forming inverters are plotted over the stabilizing period. The frequency response at Bus 6 is identifiable as the limiting case for transient performance. Referencing Fig. 3, this is potentially a result of its placement between the upper half of the power grid, which only contains load-only buses, and the lower half, which contains the five generators. This is insightful for strategic placement strategies that could eliminate the need of using advanced controls on each inverter. The optimal placement of virtual inertia devices is a high-interest area of research for frequency stabilization in power grids [34], [35]. In Fig. 7, it can be seen that the incorporation of the controlled virtual power compensation reduces the peak frequency deviation, which improves the grid resilience over the traditional droop-controlled system.

The improved resilience is evident by the H-infinity norm reduction (35.75%) shown in TABLE III. is a result of the H-infinity SOF controlled virtual power injection. This improvement is attributed to the advantage of actuating the frequency and voltage with virtual power in a way that a conventionally droop-controlled system fails. These improvements can be connected intuitively to the shorter stabilizing periods and reduced oscillation for the adjusted droop-controlled systems as seen in Fig. 7. In particular, the transient response at Bus 6 shown in Fig. 7 is a promising valuation of the proposed control methodology.

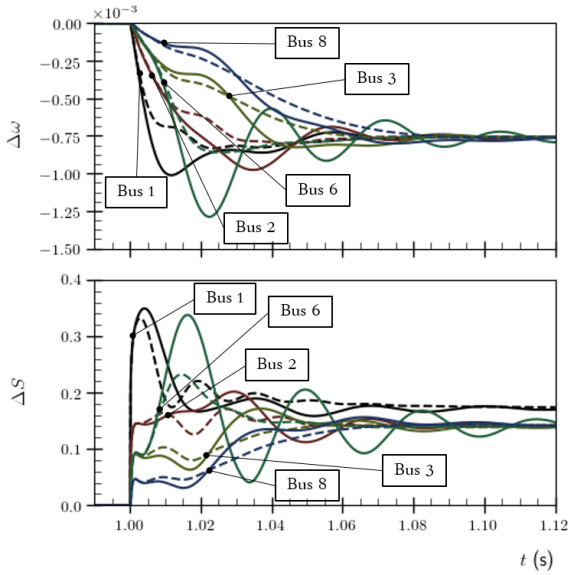

Fig. 7. Frequency response, $\Delta\omega$ (p.u.), and apparent power, $\Delta S = \sqrt{\Delta P^2 + \Delta Q^2}$ (p.u.), injection following a 5% load increase at Bus 1 for Bus 1, Bus 2, Bus 3, Bus 6, and Bus 8. Simulations are compared for traditional droop control and adjusted droop control (dashed line).

The cost for the outlined improvements, quantified by the integrated power injection over the stabilizing period ($\int \Delta S$) is minuscule. The overall energy is increased by

2.64% and only minor adjustments in the power injection over the stabilizing period are observed in Fig. 7.

VI. Conclusion

This paper introduces a novel method of virtual power injection SOF feedback control for frequency stabilization in islanded power grids. The utilization of a linearized power grid model that supports the computation of H-infinity optimal SOF controllers for grid-forming VSIs accomplishes major improvements with regard to the frequency time response and resilience of the power grid system with minimal energy cost. This is tested for a modified meshed IEEE 14 and IEEE 24-bus test system to show that the proposed H-infinity controller synthesis is scalable to practical and complex systems. A meshed topology is considered here to generalize the potential of this methodology. This method can also excel in radial topologies, where the frequency stabilization problem is simplified with the absence of inter-bus loops.

The initial analysis on a 14 and 24-bus power grid is promising. In the future, we will focus on scaling up to a larger power grid and developing reduced-order models and their synthesis with decentralized controllers. Efforts that target the optimal design and placement of virtual power controllers in sizable power grid topologies will also be studied.

References

[1] IEA, Re-powering Markets: Market design and regulation during the transition to low-carbon power systems, ser. Electricity Market Series. Paris: IEA, 2016.

[2] P. Dondi, D. Bayoumi, C. Haederli, D. Julian, and M. Suter, "Network integration of distributed power generation," J. Power Sources, vol. 106, no. 1-2, pp. 1–9, 2002.

[3] J. P. Lopes, N. Hatziargyriou, J. Mutale, P. Djapic, and N. Jenkins, "Integrating distributed generation into electric power systems: a review of drivers, challenges and opportunities," Electr. Power Syst. Res., vol. 77, no. 9, pp. 1189–1203, 2007.

[4] S. Parhizi, H. Lotfi, A. Khodaei, and S. Bahramirad, "State of the art in research on microgrids: a review," IEEE Access, vol. 3, pp. 890–925, 2015.

[5] D. E. Olivares, A. Mehrizi-Sani, A. H. Etemadi, C. A. Cañizares, R. Iravani, M. Kazerani, A. H. Hajimiragha, O. Gomis-Bellmunt, M. Saeedifard, R. Palma-Behnke et al., "Trends in microgrid control," IEEE Trans. Smart Grid, vol. 5, no. 4, pp. 1905–1919, 2014.

[6] A. Von Meier, Electric power systems: a conceptual introduction. Hoboken, NJ: John Wiley & Sons, 2006.

[7] A. Ulbig, T. S. Borsche, and G. Andersson, "Impact of low rotational inertia on power system stability and operation," IFAC Proc. Volumes, vol. 47, no. 3, pp. 7290–7297, 2014.

[8] H. Gu, R. Yan, and T. K. Saha, "Minimum synchronous inertia requirement of renewable power systems," IEEE Trans. Power Syst., vol. 33, no. 2, pp. 1533–1543, 2017.

[9] U. Tamrakar, D. Shrestha, M. Maharjan, B. Bhattarai, T. Hansen, and R. Tonkoski, "Virtual inertia: Current trends and future directions," Appl. Sci., vol. 7, no. 7, p. 654, 2017.

[10] S. D'Arco and J. A. Suul, "Virtual synchronous machines—classification of implementations and analysis of equivalence to droop controllers for microgrids," in 2013 IEEE Grenoble Conference. IEEE, 2013, pp. 1–7.

[11] R. Ofir, U. Markovic, P. Aristidou, and G. Hug, "Droop vs. virtual inertia: Comparison from the perspective of converter operation mode," in 2018 IEEE International Energy Conference (ENERGYCON). IEEE, 2018, pp. 1–6.

[12] J. Liu, Y. Miura, and T. Ise, "Comparison of dynamic characteristics between virtual synchronous generator and droop control in inverter-based distributed generators," IEEE Trans. Power Electron., vol. 31, no. 5, pp. 3600–3611, 2015.

[13] K. Sakimoto, Y. Miura, and T. Ise, "Characteristics of parallel operation of inverter-type distributed generators operated by a virtual synchronous generator," Electr. Eng. Jpn., vol. 192, no. 4, pp. 9–19, 2015.

[14] U. Markovic, Z. Chu, P. Aristidou, and G. Hug, "Fast frequency control scheme through adaptive virtual inertia emulation," in 2018 IEEE Innovative Smart Grid Technologies-Asia (ISGT Asia). IEEE, 2018, pp. 787–792.

[15] ——, "LQR-based adaptive virtual synchronous machine for power systems with high inverter penetration," IEEE Trans. Sustainable Energy, vol. 10, no. 3, pp. 1501–1512, 2018.

[16] J. M. Guerrero, L. G. De Vicuna, J. Matas, M. Castilla, and J. Miret, "A wireless controller to enhance dynamic performance of parallel inverters in distributed generation systems," IEEE Trans. Power Electron., vol. 19, no. 5, pp. 1205–1213, 2004.

[17] N. Soni, S. Doolla, and M. C. Chandorkar, "Improvement of transient response in microgrids using virtual inertia," IEEE Trans. Power Delivery, vol. 28, no. 3, pp. 1830–1838, 2013.

[18] T. L. Vandoorn, B. Meersman, L. Degroote, B. Renders, and L. Vandevelde, "A control strategy for islanded microgrids with dc-link voltage control," IEEE Trans. Power Delivery, vol. 26, no. 2, pp. 703–713, 2011.

[19] . A.-R. I. Mohamed and E. F. El-Saadany, "Adaptive decentralized droop controller to preserve power sharing stability of paralleled inverters in distributed generation microgrids," IEEE Trans. Power Electron., vol. 23, no. 6, pp. 2806–2816, 2008.

[20] M. K. Chu Cheong, H. Qian, J. Conger, D. Chen, and P. Du, "Distributed H∞ frequency control for inverter connected microgrids," in ASME 2017 Dynamic Systems and Control Conference. American Society of Mechanical Engineers Digital Collection, 2017.

[21] M. K. Chu Cheong, D. Chen, and P. Du, "Decentralized H∞ control in microgrids to mitigate renewable intermittency," in ASME 2016 Dynamic Systems and Control Conference. American Society of Mechanical Engineers Digital Collection, 2016.

[22] N. Pogaku, M. Prodanovic, and T. C. Green, "Modeling, analysis and testing of autonomous operation of an inverter-based microgrid," IEEE Trans. Power Electron., vol. 22, no. 2, pp. 613–625, 2007.

[23] H. Bevrani, Robust Power System Frequency Control. USA, NY, New York: Springer, 2009, vol. 85.

[24] S. Boyd, L. El Ghaoui, E. Feron, and V. Balakrishnan, Linear Matrix Inequalities in System and Control Theory. USA, PA, Philadelphia: SIAM, 1994, vol. 15.

[25] C. A. Crusius and A. Trofino, "Sufficient LMI conditions for output feedback control problems," IEEE Trans. Autom. Control, vol. 44, no. 5, pp. 1053–1057, 1999.

[26] J. Rubió-Masseguú, J. M. Rossell, H. R. Karimi, and F. Palacios-Quinonero, "Static output-feedback control under information structure constraints," Automatica, vol. 49, no. 1, pp. 313–316, 2013.

[27] R. H. Tütüncü, K.-C. Toh, and M. J. Todd, "Solving semidefinite-quadratic-linear programs using SDPT3," Math. Program., vol. 95, no. 2, pp. 189–217, 2003.

[28] J. Lofberg, "YALMIP: A toolbox for modeling and optimization in MATLAB," in 2004 IEEE international conference on robotics and automation (IEEE Cat. No. 04CH37508). IEEE, 2004, pp. 284–289.

[29] Information Trust Institute, "Power Systems Test Case Archive." 2013. Distributed by Illinois Center for a Smarter Electric Grid (ICSEG). https://icseg.iti.illinois.edu/power-cases.

[30] N. Hashim, N. Hamzah, M. A. Latip, and A. Sallehhudin, "Transient stability analysis of the IEEE 14-bus test system using dynamic computation for power systems (dcps)," in 2012 Third International Conference on Intelligent Systems Modelling and Simulation. IEEE, 2012, pp. 481–486.

[31] P. Iyambo and R. Tzoneva, "Transient stability analysis of the IEEE 14-bus electric power system," in AFRICON 2007. IEEE, 2007, pp. 1–9.

[32] A. H. Etemadi, E. J. Davison, and R. Iravani, "A decentralized robust control strategy for multi-DER microgrids—Part I: Fundamental concepts," IEEE Trans. Power Del., vol. 27, no. 4, pp. 1843–1853, 2012.

[33] IEEE Standard for Interconnection and Interoperability of Distributed Energy Resources with Associated Electric Power Systems Interfaces, IEEE Standard 1547, 2018.

[34] B. K. Poolla, D. Groß, and F. D¨orfler, "Placement and implementation of grid-forming and grid-following virtual inertia and fast frequency response," IEEE Trans. Power Syst., vol. 34, no. 4, pp. 3035–3046, 2019.

[35] T. Borsche and F. D¨orfler, "On placement of synthetic inertia with explicit time-domain constraints," IEEE Trans. Power Sys., 2017, Submitted. Available at https://arxiv.org/abs/1705.03244.